Journal of Applied Mechanics and Technical Physics, Vol. 47, No. 1, pp. 99–108, 2006

EFFECT OF WAVE FORMATION DURING SHOCK-WAVE COMPACTION OF POWDERS

S. P. Kiselev and V. P. Kiselev

UDC 539.374+539.26

The problem of shock-wave compaction of a metal powder enclosed in a metal container with a transverse partition is solved. A model of wave formation on the partition and in the compact adjacent to the partition is proposed; the model is based on the loss of strength in the powder due to collapsing of pores and to development of instability of the partition being compressed in the shock wave.

Key words: *shock wave, powder compaction, instability, plasticity, stresses, strains.*

Introduction. Shock-wave compaction of powders is widely used for obtaining materials with prescribed properties [1–3]. One of the drawbacks of this method is origination of various inhomogeneities in the compact. For instance, compaction of a powder with a "central body" leads to formation of a "cold" layer in the compact [3]; the reasons for origination of this layer were considered in [3–5].

The experiments performed in [6] revealed a new type of inhomogeneities, which arise in shock-wave compaction of a copper powder in a cylindrical ampoule with transverse partitions made of transformer steel. The inhomogeneities were related to wave formation in transverse partitions and in adjacent layers of compacts. Additional experiments showed that the effect of wave formation after shock-wave loading was not observed if the ampoule was filled by a solid copper sample instead of the copper powder. The effect was not observed either if the transverse partitions were made of materials other than transformer steel (copper, aluminum, stainless steel, or steel St. 20). Results of numerical simulations of powder compaction in an ampoule with a transverse partition are described in the present paper; based on these results, an explanation for the wave-formation phenomenon is proposed.

Formulation of the Problem. Figure 1 shows the schematic of powder compaction used in the experiment of [6], which was numerically simulated in the present work (in contrast to [6], only one partition is considered here, but this difference is not of principal importance). A cylindrical steel shell was filled by a copper powder (or by a mixture of copper and molybdenum powders), which was densely packed. Transverse partitions, which were thin circular plates, divided the powder into several portions for technological purposes. Powder compaction proceeded in a shock wave generated by a detonation wave excited by detonation of a high explosive (HE) on the shell surface. It turned out after compaction that wavy deformation of the partitions and adjacent compact was observed if the partitions were made of transformer steel (see Fig. 1).

The effect of detonation products was simulated by pressure applied to the upper boundary of the shell $P(x,t)$. The pressure at the detonation-wave front $x = Dt$ was found from the Chapman–Jouguet condition [7] by the formula $P_H = (2/(\gamma+1))\rho_{\text{HE}}D^2$, where ρ_{HE} is the density of the high explosive, D is the detonation velocity, and $\gamma = 3$. Behind the detonation-wave front, the pressure decreases in the centered expansion wave $Dt/2 < x < Dt$ with an adjacent region $0 < x < Dt/2$, where the pressure is constant [7]. The pressure behind the detonation-wave front is calculated by the following formula [7]:

Institute of Theoretical and Applied Mechanics, Siberian Division, Russian Academy of Sciences, Novosibirsk 630090; kiselev@itam.nsc.ru. Translated from Prikladnaya Mekhanika i Tekhnicheskaya Fizika, Vol. 47, No. 1, pp. 119–130, January–February, 2006. Original article submitted April 25, 2005.

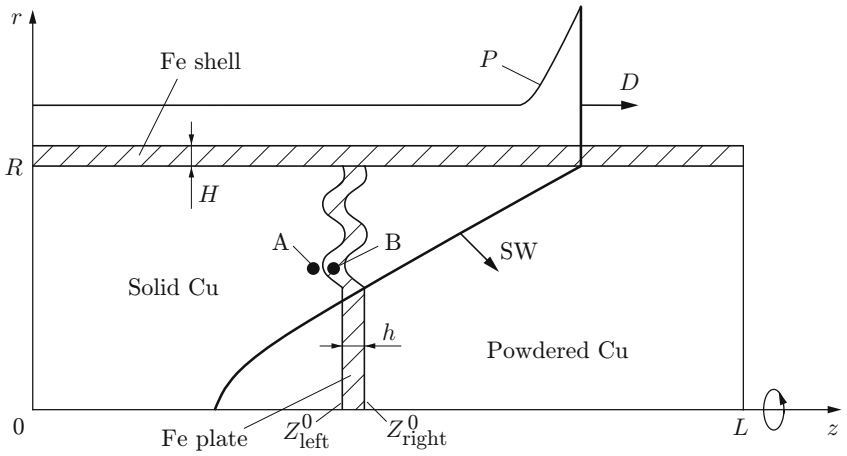

Fig. 1. Schematic of powder compaction in a cylindrical container.

$$P = P_H\Big(\frac{c}{c_H}\Big)^3, \qquad c_H = \frac{\gamma D}{\gamma+1}, \qquad c = \begin{cases} x/(2t) + D/4, & D/2 < x/t < D, \\ D/2, & x/t < D/2. \end{cases}$$

The stress–strain state of the shell and partition was calculated within the elastoplastic Prandtl–Reuss model [8].

In mathematical modeling of powder compaction, it should be borne in mind that the powder is densely packed before it is subjected to a shock wave. Then powder compaction proceeds owing to collapsing of pores and no slipping of powder particles is observed. Loads considered in the present paper imply complete collapsing of pores in the shock-wave front and formation of strong bonds between powder particles. Powder compaction by a shock wave, therefore, can be described by a model of a porous elastoplastic material [9, 10], and the compact being formed can be described by the Prandtl–Reuss model.

The problem involves several contact boundaries, namely, the shell–powder, partition–powder, and partition–shell boundaries. An ideal contact condition was imposed on all contact boundaries: displacements of the corresponding points of two contacting bodies are identical, and the forces of interaction are identical in magnitude and opposite in direction. In the present case, this approximate condition is valid because the stress of dry friction between the contacting bodies under loads [6] $P \approx 2$ GPa is of the order of the yield strength of the material: $\sigma_f = fP \sim Y_{\text{s}}$. The numerical solution of the problem was based on a "cross" finite-difference scheme adapted in [8] to calculations of elastoplastic media. A predictor–corrector-type algorithm was used to calculate the contact boundary of two contacting bodies with an ideal contact. The predictor stage involved calculations of new positions and velocities of the boundaries of each body without allowance for the influence of the second body. After that, at the corrector stage, the resultant boundaries were corrected with allowance for the ideal contact conditions. The velocity of the contact boundary was found from the law of conservation of momentum in an inelastic collision of contacting boundary cells with velocities obtained at the predictor stage. Conditions of an ideal contact can be demonstrated to be satisfied in this case. The algorithm was previously used for a one-dimensional case (see [11]) and is extended to a two-dimensional case in the present work.

Mathematical Model of the Powder. The behavior of the powder under shock-wave loading was simulated within the framework of the mathematical model of a porous elastoplastic material, which was proposed in [9, 10]. The equations of continuity, motion, and energy have the form

$$\frac{\partial\rho}{\partial t} + \nabla_i \rho v_i = 0, \quad \rho = \rho_{\text{s}} m_2, \quad m_1 + m_2 = 1, \quad \rho\frac{dv_i}{dt} = \nabla_j \sigma_{ij}, \quad \nabla_i = \frac{\partial}{\partial x_i},$$

$$\frac{d}{dt} = \frac{\partial}{\partial t} + v_i\nabla_i, \qquad \rho\frac{dE_S}{dt} = \sigma_{ij}\dot{\varepsilon}_{ij}, \qquad \dot{\varepsilon}_{ij} = \frac{1}{2}\left(\nabla_i v_j + \nabla_j v_i\right), \tag{1}$$

$$\sigma_{ij} = -P\delta_{ij} + S_{ij}, \qquad m_1 = (4/3)\pi a^3 n, \qquad i,j = 1,2,3,$$

where a and n are the pore radius and concentration, m_1 is the volume concentration of pores (porosity), m_2 is the volume concentration of the material, ρ is the mean density, σ_{ij} and $\dot{\varepsilon}_{ij}$ are the mean stress tensor and strain-rate tensor, v_i is the ith component of velocity, E_S is the specific internal energy, P is the pressure, and S_{ij} is the stress-tensor deviator.

System (1) was closed by the equation of state of the porous body

$$\dot{P} = \dot{P}_{\text{cold}} + \dot{P}_{\text{heat}}, \qquad \dot{P}_{\text{cold}} = -K\dot{\varepsilon}^{\text{e}}_{kk}, \qquad P_{\text{heat}} = \Gamma\rho E_{\text{heat}},$$
$$E_S = E_{\text{cold}} + E_{\text{heat}}, \qquad E_{\text{cold}} = (K_1(\varepsilon^{\text{e}}_{kk})^2/2 + \mu_1 e^{\text{e}}_{ij}e^{\text{e}}_{ij})/\rho, \qquad e_{ij} = e^{\text{e}}_{ij} + e^{\text{p}}_{ij}, \tag{2}$$

where K_1 and μ_1 are the mean elastic moduli of volume compression and shear of the porous material.

The stress-tensor deviator is determined by Hooke's law

$$\overset{\nabla}{S}_{ij} = 2\mu\dot{e}_{ij}, \qquad \dot{e}_{ij} = \dot{\varepsilon}_{ij} - (1/3)\dot{\varepsilon}_{kk}\delta_{ij} \tag{3}$$

in the region of elastic strains $(3/2)S_{ij}S_{ij} < Y^2$ and by the Prandtl–Reuss equations

$$\dot{e}_{ij} = \overset{\nabla}{S}_{ij}/(2\mu) + \dot{\lambda}S_{ij}, \qquad (3/2)S_{ij}S_{ij} = Y^2,$$
$$\overset{\nabla}{S}_{ij} = \dot{S}_{ij} - \omega_{ik}S_{kj} - \omega_{jk}S_{ki}, \qquad \omega_{ij} = (v_{i,j} - v_{j,i})/2 \tag{4}$$

in the plastic region (the symbol ∇ indicates the Jaumann derivative and the dot over the symbol means the substantial derivative with respect to time). In system (1)–(4), P_{cold} and P_{heat} are the cold and heat pressures, E_{cold} and E_{heat} are the cold and heat energies, respectively, K is the modulus of volume compression, μ is the shear modulus, Y is the yield strength, Γ is the Grüneisen coefficient, and ω_{ij} is the antisymmetric tensor of velocity of revolution of the medium; each of the subscripts i, j, and k runs through the values of 1, 2, and 3; summation is performed over repeated subscripts; the subscript after the comma indicates the derivative with respect to the corresponding coordinate; the superscripts "e" and "p" refer to elastic and plastic strains, respectively.

The yield surface of the porous material has the form

$$Y^2 = \begin{cases} Y_{\text{s}}^2 m_2^2 - (9/4)P^2 m_1, & |P| \leqslant |P_0|, \\ Y_{\text{s}}^2 m_2 m_{\text{e}}^2, & |P_0| < |P| \leqslant |P_*|, \\ 0, & |P| > |P_*|, \end{cases} \tag{5}$$

$$m_{\text{e}}^2 = \frac{1+m_1^2}{m_2} - 2\,\frac{m_1}{m_2}\,\cosh\frac{3P}{2Y_{\text{s}}}, \qquad m_{\text{e}} + m_{\text{p}} = 1,$$

where $|P_*| = (2/3)Y_{\text{s}}\ln(1/m_1)$, $|P_0| = (2/3)Y_{\text{s}}(1-m_1)$, and m_{e} and m_{p} are the fractions of the cell volume in the elastic and plastic states, respectively. It follows from Eqs. (5) that the yield strength decreases with increasing pressure $|P|$ and vanishes at $|P| = |P_*|$. Note that the yield surface constructed by Eqs. (5) is close to Garson's yield surface [12].

For $|P| < |P_0|$, elastic loading (unloading) occurs, and the following formulas are valid:

$$K = K_1 = K_{\text{s}}m_2\Big/\Big(1 + \frac{m_1}{2}\,\frac{1+\nu}{1-2\nu}\Big), \qquad \mu = \mu_1 = \frac{\mu_{\text{s}}m_2}{1+m_1/2}, \qquad \dot{\varepsilon}^{\text{e}}_{kk} = -\frac{\dot{\rho}_{\text{s}}}{\rho_{\text{s}}} \tag{6}$$

(K_{s} and μ_{s} are the elasticity moduli of the solid material; ν is Poisson's ratio). For $|P_0| < |P| < |P_*|$, a plastic zone is formed around the pore, the strains acquire an elastoplastic character, and the following formulas are valid:

$$K = K_2 = K_{\text{s}}m_2\Big/\Big(1 + \frac{1+\nu}{3(1-2\nu)}\,\frac{Y}{|P|}\,m_{\text{p}}m_2\Big), \qquad \mu = \mu_2 = \frac{\mu_{\text{s}}m_{\text{e}}}{m_{\text{e}}/m_2 + m_{\text{p}}/2},$$
$$e^{\text{e}}_{ij} = S_{ij}/(2\mu_1), \qquad \dot{\varepsilon}^{\text{e}}_{kk} = (K_2/K_1)\dot{\varepsilon}_{kk}, \qquad \dot{\varepsilon}_{kk} = -\dot{\rho}/\rho. \tag{7}$$

Equations (7) refer to the case of loading ($P\dot{P} > 0$). Under unloading ($P\dot{P} < 0$), the material is described by Eqs. (6) to a certain extent; subsequent loading from this state occurs in an elastic manner. If $|P| > |P_*|$, the pores lose their stability and collapse. In this case, the yield strength (5) vanishes; hence, the components of the stress-tensor deviator are also equal to zero ($S_{ij} = 0$), and the equations of the spherical part of the stress tensor are determined by the first three equations in (2), which imply that

$$K = K_1, \qquad \Gamma = \Gamma_s K/K_1, \qquad \dot{\varepsilon}^e_{kk} = \dot{m}_2/m_2 - \dot{\rho}/\rho, \tag{8}$$

where Γ_s is the Grüneisen coefficient of the solid material.

It follows from the equation $m_1 + m_2 = 1$ that the volume concentration of the material increases ($\dot{m}_2 > 0$) in the case of pore collapsing ($\dot{m}_1 < 0$). The value of m_2 is found from the Carroll–Holt equation [13], which has the following form with inertial terms being neglected [10]:

$$P = \frac{2}{3} Y_s \ln \frac{\alpha}{\alpha - 1} - \frac{4}{3} \eta \frac{\dot{\alpha}}{\alpha(\alpha - 1)} \tag{9}$$

(this equation contains an auxiliary variable $\alpha = 1/m_2$; η is the material viscosity).

The specific heat energy E_{heat} is calculated as [10]

$$E_{\text{heat}} = E_1 + E_2,$$
$$E_1 = \frac{4\eta}{3\rho_s} \int \frac{\dot{\alpha}^2\, dt}{\alpha(\alpha - 1)}, \qquad E_2 = \frac{2Y_s}{3\rho_s} \Big\{ \alpha_0 \ln \frac{\alpha_0}{\alpha} - (\alpha_0 - 1) \ln \frac{\alpha_0 - 1}{\alpha - 1} + (\alpha_0 - \alpha) \ln \frac{\alpha}{\alpha - 1} \Big\} \tag{10}$$

(E_1 and E_2 are the mean values of dissipated energy in the case of viscous and plastic collapsing of pores, respectively).

Note, if the porosity equals zero ($m_1 = 0$), system (1)–(10) coincides with the system of equations in the Prandtl–Reuss model. For this reason, the behavior of the solid elastoplastic material is described by Eqs. (1)–(10) with $m_1 = 0$.

The above-described model was first proposed in [9]. Based on this model, problems of the impact of solid projectiles on porous iron and aluminum plates were solved [14, 15], and good agreement between the predicted and experimentally measured shock-wave profiles was reached. The transition from regular to irregular interaction of oblique shock waves in an aluminum powder was examined in [16] with the use of this model. The boundaries of the transition from one interaction mode to the other are consistent with the experimental results of [17]. Thus, it was demonstrated in [14–16] that the present model offers a correct description of shock-wave processes in porous materials and powders.

Results of Calculating Powder Compaction in a Cylindrical Container with a Transverse Partition. Numerical calculations were performed for an axisymmetric case; the geometrical and physical parameters in the calculations followed the test conditions of [6]. The cylindrical steel shell filled by the powder had the following geometrical and mechanical parameters: length $L = 6$ cm, radius $R = 1.6$ cm, thickness $H = 0.2$ cm, volume compression modulus $K_s = 1.7 \cdot 10^2$ GPa, shear modulus $\mu_s = 0.8 \cdot 10^2$ GPa, and yield strength $Y_s = 0.3$ GPa. The transverse partition was a circular plate of radius $R = 1.6$ cm and thickness $h = 0.04$ cm, which was placed at a distance $l_1 = 2.4$ cm from the left end of the shell (see Fig. 1). The shell length and radius in the calculations were chosen to be their halved values used in the experiment [6]. This difference is of no principal importance; such values were chosen to have a moderate size of the computational domain. The transverse partition was made of transformer steel [6], which is much more brittle that ordinary steel; therefore, the yield strength in the calculations was chosen to be $Y_s = 1.2$ GPa, and the elastic moduli had the same values as those for the steel shell. The copper powder was simulated by a porous body with an initial porosity $m_1^0 = 0.35$ and a pore radius $a^0 = 20$ μm. The following parameters of copper were used in the calculations: $\rho_s = 8.9 \cdot 10^3$ kg/m^3, $K_s = 1.39 \cdot 10^2$ GPa, $\mu_s = 0.46 \cdot 10^2$ GPa, $Y_s = 0.2$ GPa, and $\eta = 10^3$ Pa $\cdot$ sec.

At the time $t = 0$, the detonation wave starts propagating along the shell surface from left to right with a velocity $D = 3.6$ km/sec; the pressure of detonation products at the Chapman–Jouguet point is $P_H = 2.9$ GPa. An oblique shock wave penetrates into the shell and then into the powder and the plate. At the initial time $t = 0$, the plate surface is assumed to be subjected to a small perturbation, so that the left Z_{left} and right Z_{right} contact boundaries between the plate and the powder obey the equations

$$Z^0_{\text{left}} = l_1 + \delta a \sin(2\pi r/\lambda), \qquad Z^0_{\text{right}} = Z^0_{\text{left}} + h \qquad (\delta a \ll h \ll \lambda), \tag{11}$$

where $\delta a = 12.5$ μm is the perturbation amplitude and $\lambda = 2$ mm is the wavelength; the superscript 0 at the coordinates of the contact boundaries indicates the time $t = 0$. In solving the problem, we have to determine the evolution of this perturbation and the coordinates of the contact boundaries $Z_{\text{left}}(t)$ and $Z_{\text{right}}(t)$ for $t > 0$.

The isobars in the powder, plate, and shell in the region 0.20 cm $< z <$ 2.65 cm at the time $t = 12.8$ μsec are plotted in Fig. 2a. The pores collapse behind the shock-wave front, and the isolines of porosity are similar to

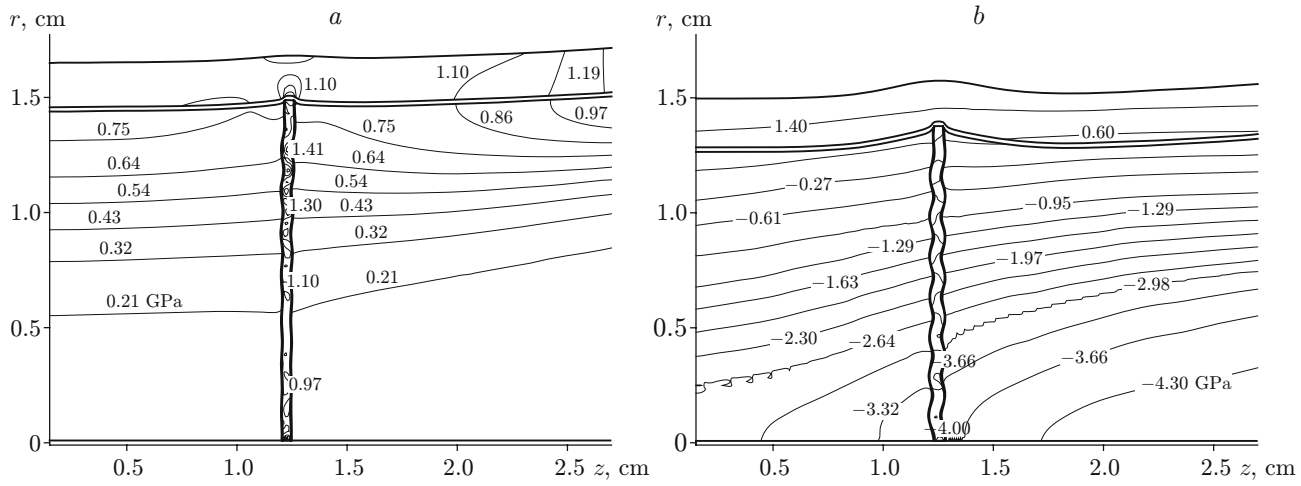

Fig. 2. Isobars in the powder, plate, and shell at $t = 12.8$ (a) and 32 μsec (b).

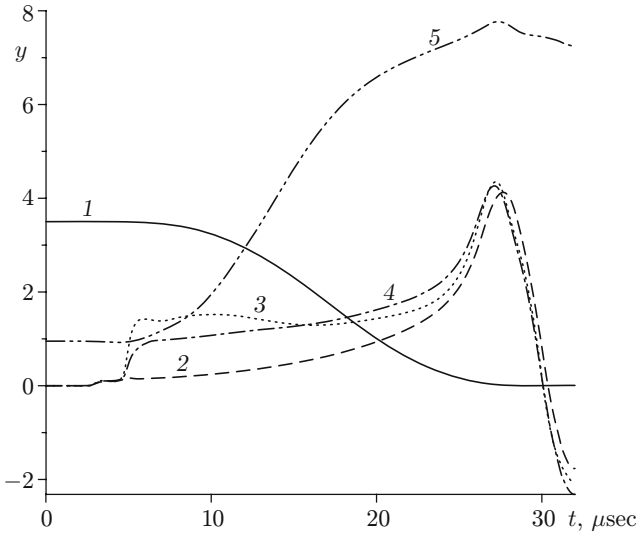

Fig. 3. Time evolution of various parameters indicated at the y axis: porosity $m_1|_{\rm A}$ (1), pressure in the powder $P|_{\rm A}$ (GPa) (2), stress in the plate $(-\sigma_r)|_{\rm B}$ (GPa) (3), pressure in the plate $P|_{\rm B}$ (GPa) (4), and dimensionless amplitude of the plate perturbation $\delta Z_{\rm left}/\delta Z^0_{\rm left}$ (5).

the isobars in the powder. The shock-wave width is determined by the pore-collapse time; hence, the shock wave in the powder is strongly "blurred." Figure 2b shows the isobars at the time $t = 32$ μsec, when the shock wave has already been reflected from the centerline and reached the shell surface, whereas an expansion wave has been formed near the axis. The pores have been already collapsed by that time, and the plate shape remains unchanged in the sequel. Shock-wave loading is seen to induce a significant wavy deformation of the plate surface.

Figure 3 shows the porosity m_1 and pressure P in the powder at the point A, the dimensionless amplitude of the plate perturbation $\delta Z_{\rm left}/\delta Z^0_{\rm left}$, the pressure P, and the stress σ_r in the plate at the point B, where $\delta Z_{\rm left}/\delta Z^0_{\rm left} = (Z_{\rm left}(t)|_{\max} - Z_{\rm left}(t)|_{\min})/(2\delta a)$, as functions of the time t. The points A and B are located on different sides of the powder–plate contact boundary [$z = Z_{\rm left}(t)$ and $r = 0.87$ cm] (see Fig. 1). The growth of plate-surface perturbations is observed only during the pore collapse. Note that the perturbations do not grow if the loss of strength of the copper powder in the case of the pore collapse is ignored in the equations for the porous body and assume that $Y = Y_{\rm s} = {\rm const}$ instead of Eq. (5). Curves 2 and 3 in Fig. 4 show the contact boundaries of the plates $Z_{\rm left} = Z_{\rm left}(r)$ at the time $t = 32$ μsec, which were obtained in two calculations under identical loading

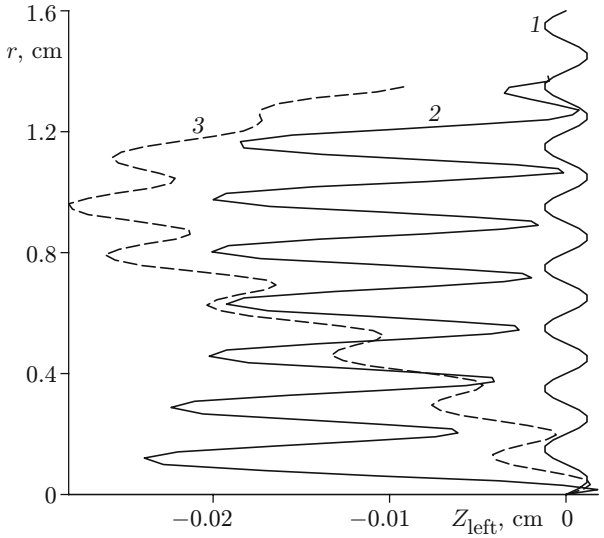

Fig. 4. Plate–powder contact boundaries $Z_{\text{left}}(r)$ at the times $t = 0$ (curve 1) and 32 μsec for first and second calculations (curves 2 and 3, respectively).

conditions (curve 1 shows the position of the plate at the initial time). The full system (1)–(10) was solved in the first calculation (curve 2). The second calculation (curve 3) was based on the same system of equations with $Y = Y_{\text{s}} = \text{const}$ instead of Eq. (5). The amplitude of perturbations in the second case changes insignificantly, though the plate experiences a greater deformation than in the first case. The latter is related to focusing of the shock wave converging toward the axis of symmetry, which leads to significant nonuniformity in the fields of velocities and displacements in the powder [18].

Discussion of Results. As was noted above, the growth of perturbations of the plate and the associated wave formation start behind the shock-wave front in the powder, where the pore collapse and the loss of strength of the powder occur. The plate behind the shock-wave front experiences radial compression and is surrounded by the powder whose mechanical properties are similar to the properties of a liquid. As a result, instability starts developing in the plate, and the perturbation amplitude increases. The adjacent powder in this case does not prevent the growth of perturbations. Velocity perturbations arise in the powder under the action of the plate, and the powder is displaced from the maximums to the minimums of pressure perturbations. If the yield strength is constant, elastic stresses arise in the powder and prevent the growth of perturbations in the plate.

Let us evaluate the wavelength and the characteristic time of growth of perturbations of the plate surrounded by the powder in which the components of the stress-tensor deviator are equal to zero because of the equality $Y = 0$. We consider a model problem on stability of a plate subjected to radial compression and immersed into an ideal incompressible liquid. The formulation of this problem is similar to the problem of motion of a plate floating on the liquid surface under the action of pressure in the liquid [19, 20]. Assuming that plate deformations are small and neglecting nonlinear terms, we rewrite the equations of motion of the plate and liquid from [20] in the form

$$\rho_{\text{s}} \frac{\partial^2 \zeta}{\partial t^2} = -\frac{D}{h} \Delta^2 \zeta + \tilde{\sigma}_r \frac{\partial^2 \zeta}{\partial r^2} + \Big(\frac{\partial \tilde{\sigma}_r}{\partial r} + \frac{\tilde{\sigma}_r}{r} \Big) \frac{\partial \zeta}{\partial r} + \frac{2P'}{h}, \qquad D = \frac{Eh^3}{12(1-\nu^2)},$$

$$\Delta \varphi' = 0, \qquad P' = -\rho_0 \frac{\partial \varphi'}{\partial t}\Big|_{z=Z}, \qquad \frac{\partial \zeta}{\partial t} = \frac{\partial \varphi'}{\partial z}\Big|_{z=Z}, \tag{12}$$

where φ' and P' are perturbations of the potential and pressure, respectively, ρ_0 is the liquid density, $\zeta = Z - Z^0$ is the amplitude of the perturbation of the mid-surface of the plate, ρ_{s}, E, and ν are the density, Young's modulus, and Poisson's ratio of the plate, respectively, and $\tilde{\sigma}_r$ is the mean radial stress in the plate. The last two equations in (12) express the equality of the normal stresses and velocities at the plate–liquid contact boundary. The plate displacement $\partial\zeta/\partial t$ induces an increase in pressure on one side of the plate and an identical decrease in pressure on the other side; therefore, the last term in the first equation in (12) was doubled, as compared to the corresponding

term in [20]. Let us consider the behavior of perturbations with a small wavelength $\lambda \ll R$, where R is the plate radius. In this case, the following inequalities are valid:

$$\frac{1}{r}\frac{\partial\zeta}{\partial r}\Big/\frac{\partial^2\zeta}{\partial r^2} \sim \frac{\lambda}{R} \ll 1, \quad \frac{\partial\tilde{\sigma}_r}{\partial r}\frac{\partial\zeta}{\partial r}\Big/\Big(\tilde{\sigma}_r\frac{\partial^2\zeta}{\partial r^2}\Big) \sim \frac{\tilde{\sigma}_r}{\tilde{\sigma}_r}\frac{\lambda}{R} \ll 1, \quad \frac{\tilde{\sigma}_r}{r}\frac{\partial\zeta}{\partial r}\Big/\Big(\tilde{\sigma}_r\frac{\partial^2\zeta}{\partial r^2}\Big) \sim \frac{\lambda}{R} \ll 1.$$

Leaving derivatives of the highest order in Eqs. (12), we obtain

$$\rho_{\rm s}\frac{\partial^2\zeta}{\partial t^2} = -\frac{D}{h}\frac{\partial^4\zeta}{\partial r^4} + \tilde{\sigma}_r\frac{\partial^2\zeta}{\partial r^2} - \frac{2\rho_0}{h}\frac{\partial\varphi'}{\partial t}\Big|_{z=0}, \qquad \frac{\partial^2\varphi'}{\partial r^2} + \frac{\partial^2\varphi'}{\partial z^2} = 0, \qquad \frac{\partial\zeta}{\partial t} = \frac{\partial\varphi'}{\partial z}\Big|_{z=0}, \tag{13}$$

where the unperturbed plate surface is placed into the cross section $z = 0$. The condition of continuity of normal stresses on the plate surface and small angles of plate-surface deviation from the vertical axis yield the equal values of stresses $\sigma'_z = \sigma_z$. Assuming that $\sigma'_z = -P'$ in the liquid, we find the pressure $P = P' + S_z$ and the radial stresses in the plate $\sigma_r = -P' + S_r - S_z$. The calculations show that the components of the stress-tensor deviator averaged over the plate thickness are $\tilde{S}_r - \tilde{S}_z = -\xi Y_{\rm s}$ ($\xi \sim 1$), and the pressure in the powder is $P' \ll Y_{\rm s}$. It follows from here that the mean radial stress in the plate remains almost constant ($\tilde{\sigma}_r \approx -\xi Y_{\rm s}$, where $\xi \approx 1$), which is validated by the calculations (see curve 3 in Fig. 3). Representing, for $z < 0$, the solution of Eqs. (13) in the form $\zeta = \zeta_0 \exp(ikr - i\omega t)$, $\varphi' = \varphi_0 \exp(kz + ikr - i\omega t)$, and taking into account that $\tilde{\sigma}_r \approx -Y_{\rm s}$, we find

$$\omega^2 = \frac{(D/h)k^4 - \xi Y_{\rm s}k^2}{\rho_{\rm s} + 2\rho_0/(kh)},$$

where ω is the frequency and $k = 2\pi/\lambda$ is the wavenumber of perturbations. It follows from here that perturbations with the wavelength $\lambda > \lambda_*$ are exponentially increasing as

$$\zeta \sim \zeta_0 \exp\frac{t}{\tau}, \qquad \tau \approx \frac{\lambda}{2\pi}\Big/\sqrt{\frac{Y_{\rm s}(1-(\lambda_*/\lambda)^2)}{\rho_{\rm s}(1+2\rho_0/(\rho_{\rm s}kh))}}, \qquad \lambda_* = 2\pi\sqrt{\frac{D}{\xi Y_{\rm s}h}}. \tag{14}$$

This formulation of the problem on dynamic instability of the plate is similar to the problem formulated in [21] where stability of an elastic rod under pulsed loading was considered. Following [21], we find the perturbation wavelength corresponding to the lowest growth time: $\tilde{\lambda} = \sqrt{2}\,\lambda_*$. Note that a similar mechanism of wave formation during explosive welding, which was related to the loss of stability of the material in the contact region owing to residual compressive stresses, was considered in a simplified model in [22]. In particular, in contrast to the present work, Godunov and Sergeev-Al'bov [22] studied the loss of stability of a compressed rod bordering on an elastic half-plane. A problem in a formulation similar to that in [22] was solved numerically on the basis of the Maxwellian nonlinear elastoplastic model in [23]. Deformation of a plate under the action of a pressure pulse moving over the plate surface was considered. This problem allowed modeling physical parameters in the contact region in the case of explosive welding of two plates [22]. As a result, residual compressive stresses leading to bending of the entire plate were found, but no wave formation in the plate was revealed by calculations.

Using Eqs. (14), we can find the numerical values of the critical perturbation wavelength λ_* and the characteristic time of perturbation growth τ. It follows from the second equation in (12) that the cylindrical rigidity of the plate D in the case of elastic deformation is proportional to Young's modulus. The calculations show, however, that simultaneous compression and bending of the plate lead to elastoplastic deformations of the latter. One part of the plate experiences additional extension owing to bending and is elastically deformed with a modulus $E = E_{\rm e}$, whereas the other part of the plate experiences additional compression and is plastically deformed with a modulus $E = E_{\rm p}$. The distributions of radial stresses $\sigma_r(z)$ calculated in three cross sections over the plate thickness (Fig. 5) support these assumptions. Therefore, instead of Young's modulus, the second equation in (12) should have the mean modulus E_k, which takes into account the elastoplastic character of plate deformation. There are different theories for calculating E_k [24]; in what follows, we use the Engesser–Kármán model [24]. Note that the simplified equation for the plate [first equation in (13)] coincides with the equation for the rod; therefore, in determining the mean modulus E_k, we use the corresponding formula for the rod with a rectangular cross section in the Engesser–Kármán model [24]: $E_k = 4E_{\rm e}E_{\rm p}/(\sqrt{E_{\rm e}} + \sqrt{E_{\rm p}})^2$. The radial stresses in the plate are the sum of the mean and moment stresses related to plate bending [25]:

$$\sigma_r = \frac{\tilde{E}}{(1-\nu^2)}\varepsilon_r^0 - \frac{\tilde{E}z}{(1-\nu^2)}\frac{\partial^2\zeta}{\partial r^2}$$

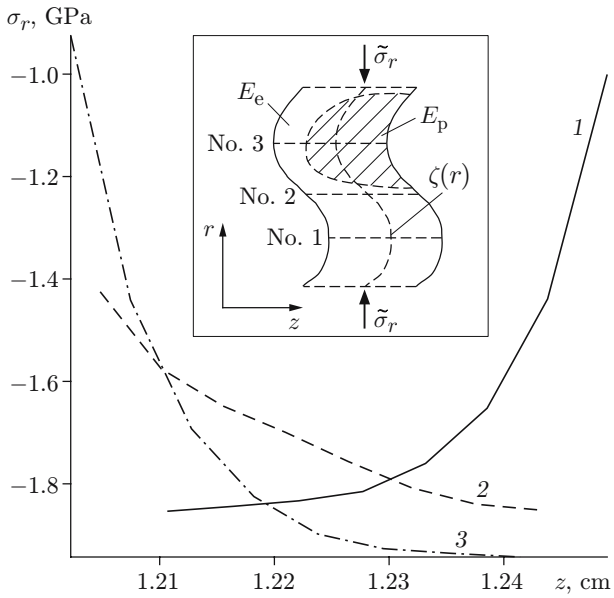

Fig. 5. Stress distribution $\sigma_r(z)$ in the plate at the time $t = 12.8$ μsec for cross sections $r = 0.82$ (curve 1), 0.87 (curve 2), and 0.91 cm (curve 3); the corresponding cross sections Nos. 1–3 are shown in the inset.

(the minus sign in the second term is conditioned by the choice of the coordinate system), where $\varepsilon_r^0 < 0$ is the strain of the plate mid-surface and $\tilde{E}$ is the local modulus. Differentiating the left and right sides of this expression with respect to z, we obtain a formula for determining the local modulus $\tilde{E}$ from a preset stress distribution $\sigma_r(z)$:

$$\tilde{E} = (1-\nu^2)\,\frac{\partial \sigma_r}{\partial z} \Big/ \frac{\partial^2 \zeta}{\partial r^2}.$$

By means of numerical calculations, we find the plate curvature for $r = 0.91$ cm, which corresponds to cross section No. 3 in the insert in Fig. 5: $\partial^2\zeta/\partial r^2 \approx 2 \cdot 10^2$ 1/m. From the stress distribution $\sigma_r(z)$ in this cross section (curve 3 in Fig. 5), we find that the material on the left boundary of the plate is deformed elastically [$\partial\sigma_r/\partial z \approx 10^4$ GPa/m and $E_e = \tilde{E}(Z_{\text{left}}) = 50$ GPa]. The same cross section on the right boundary of the plate experiences plastic deformation of the material; hence, we have $\partial\sigma_r/\partial z \approx 2 \cdot 10^2$ GPa/m and $E_p = \tilde{E}(Z_{\text{right}}) = 1$ GPa. Substituting these values into the formula for the mean modulus, we obtain $E_k = 4$ GPa. Determining the cylindrical rigidity by the formula $D = E_k h^3/(12(1-\nu^2))$, we use Eq. (14) to find the minimum wavelength of unstable perturbations $\lambda_* \approx 1.3$ mm and the characteristic time of growth $\tau \approx 1.56$ μsec of perturbations with a wavelength $\lambda = 2$ mm. In the experiment of [6], the wavelength of perturbations in the plate was $\lambda_0 \approx 2.5$ mm, which was close to the above-estimated wavelength of the most rapidly growing perturbations $\tilde{\lambda} = \sqrt{2}\,\lambda_* \approx 1.82$ mm.

Numerical calculations yield a similar value $\lambda_* \approx 1$ mm, and the value $\tau \approx 6$ μsec for $\lambda = 2$ mm, which is greater by a factor of 4. Apparently, the difference in the values of τ is caused by the neglect of powder compressibility in the simplified model described by Eqs. (12). As is seen from Fig. 3, the change in powder density in the calculations during the time $\tau \approx 6$ μsec is approximately 30%.

Three sets of calculations were performed to study the growth of perturbations of the plate depending on the character of the initial perturbation and strength parameters of the plate.

In the first set of calculations, we changed the perturbation wavelength λ, and the initial perturbation amplitude remained constant: $\delta a = 12.5$ μm. The calculation results are plotted in Fig. 6, which shows the dimensionless amplitude of the perturbation in the plate $\zeta/\zeta_0 = (Z_{\text{left}}(t)|_{\max} - Z_{\text{left}}(t)|_{\min})/(2\,\delta a)$ as a function of the time t for different wavelengths λ. It is seen that perturbations with wavelengths $\lambda < 1$ μm do not grow. Perturbations with λ in the range of 3 to 4 mm have the maximum growth rate, and then the perturbation growth rate decreases with increasing wavelength.

In the second set of calculations, we changed the yield strength of the plate in the range 0.2 GPa $< Y_s <$ 1.2 GPa, and the remaining parameters (λ and δa) were constant. The numerical calculations showed that the

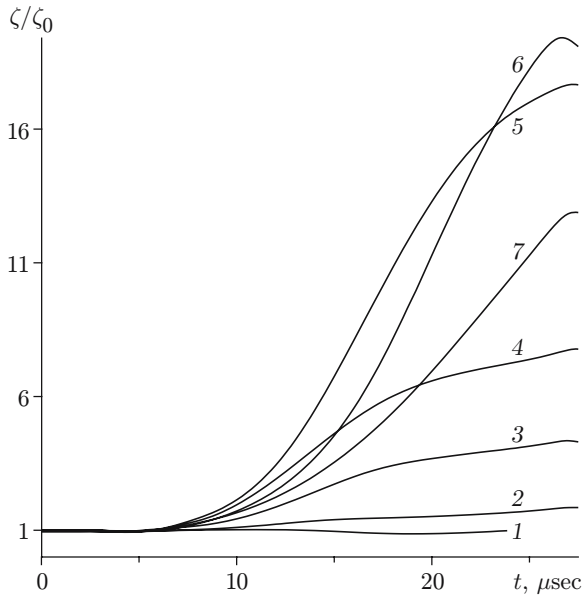

Fig. 6. Dimensionless amplitude of the perturbation ζ/ζ_0 of the plate versus the time t calculated for different perturbation wavelengths: $\lambda = 0.7$ (1), 1 (2), 1.5 (3), 2 (4), 3 (5), 4 (6), and 5 mm (7).

dependence of the characteristic growth time of the perturbation on the yield strength has the form $\tau \sim 1/\sqrt{Y_s}$, which agrees with the second formula in (14).

In the third set of calculations, we considered the growth of perturbations as a function of the amplitude of the initial perturbation of the plate with a constant perturbation wavelength. The maximum perturbation amplitude turned out to be independent of the amplitude of initial perturbations of the plate δa in a fairly wide range $0.02 < 2\pi\,\delta a/\lambda < 0.16$, where the perturbation wavelength was $\lambda = 2$ mm. If there were no perturbations of the plate ($\delta a = 0$) at the initial time $t = 0$, they did not arise at later times $t > 0$ either. Apparently, wave formation in a plate made of transformer steel is associated with the presence of large-scale inhomogeneities that act as sources of perturbations in the plate. The issue of the source of initial perturbations is outside the scope of the present work, as it requires some additional studies. If perturbation have already appeared, however, they are amplified owing to development of plate instability in the compression wave and simultaneous softening of the powder due to pore collapsing.

The authors are grateful to S. K. Godunov and V. I. Mali for discussing the formulation of the problem and intermediate and final results of calculations.

This work was supported by the Russian Foundation for Basic Research (Grant No. 04-01-00894-a).

REFERENCES

1. A. B. Sawaoka (ed.), *Shock Waves in Materials Science*, Springer-Verlag, Hong Kong–Barcelona–Budapest (1993).
2. R. Prummer, *Explosivverdichtung Pulvriger Substanzen*, BRD, Springer-Verlag (1987).
3. V. F. Nesterenko, *Pulsed Loading of Heterogeneous Materials* [in Russian], Nauka, Novosibirsk (1992).
4. N. A. Kostyukov, "Physical causes and mechanisms of the formation of boundary regions in the two-dimensional explosive compaction of powdered materials," *J. Appl. Mech. Tech. Phys.*, **32**, No. 6, 967–974 (1991).
5. A. E. Buzjurkin and S. P. Kiselev, "On appearance of "cold" layer in explosive consolidation of powders," *Shock Waves*, **10**, No. 3, 159–165 (2000).
6. V. I. Mali, A. N. Kalinin, and S. A. Sergeev, "Heat conduction of copper–molybdenum explosive compacts," *Combust., Expl., Shock Waves*, **39**, No. 1, 108–111 (2003).
7. F. A. Baum, L. P. Orlenko, K. P. Stanyukovich, et al., *Physics of Explosion* [in Russian], Nauka, Moscow (1975).

8. M. L. Wilkins, "Calculation of elastoplastic flows," in: B. Alder, S. Fernbach, and M. Retenberg (eds.), *Methods of Computational Physics*, Vol. 3, Academic Press, New York (1964).
9. S. P. Kiselev, "Elastoplastic model of deformation of a porous material," in: *Filtration of Multiphase Media* (collected scientific papers) [in Russian], Inst. of Theor. and Appl. Mech., Sib. Div., USSR Acad. of Sci. (1991), pp. 151–166.
10. S. P. Kiselev, G. A. Ruev, A. P. Trunev, et al., *Shock-Wave Processes in Two-Component and Two-Phase Media* [in Russian], Nauka, Novosibirsk (1992).
11. A. I. Gulidov and I. I. Shabalin, "Numerical implementation of boundary conditions in dynamic contact problems," Preprint No. 12, Inst. Theor. and Appl. Mech., Sib. Div., Russian Acad. of Sciences, Novosibirsk (1987).
12. A. L. Garson, "Continuum theory of viscous failure, caused by pore formation and growth. Chapter 1: Yield criteria and yield laws for porous plastic media," *Trans. ASME, Ser. Theor. Found. Eng. Calc.*, No. 1, 1–17 (1977).
13. M. M. Carroll and A. C. Holt, "Static and dynamic pore-collapse relations for ductile porous materials," *J. Appl. Phys.*, **43**, No. 4, 1626–1635 (1972).
14. S. P. Kiselev, "On propagation of a shock wave in a porous material upon collision of plates," *Combust., Expl., Shock Waves*, **31**, No. 4, 473–477 (1995).
15. S. P. Kiselev, "Numerical simulation of propagation of elastoplastic waves in a porous material," Preprint No. 6, Inst. Theor. and Appl. Mech., Sib. Div., Russian Acad. of Sciences, Novosibirsk (1994).
16. S. P. Kiselev and A. E. Buzjurkin, "Shock-wave processes in metal powders," *Fiz. Mezomekh.*, **3**, No. 6, 51–63 (2000).
17. N. A. Kostyukov, "Effect of the initial density of a substance on the conditions of oblique collision of shock waves," *J. Appl. Mech. Tech. Phys.*, **18**, No. 3, 379–383 (1977).
18. A. E. Buzjurkin and S. P. Kiselev, "Powder compaction in the axisymmetric case," *Mater. Phys. Mech.*, **7**, No. 1, 17–22 (2004).
19. L. D. Landau and E. M. Lifshitz, *Theory of Elasticity*, Pergamon Press, Oxford–New York (1970).
20. S. P. Kiselev and A. P. Trunev, "Dynamic damage and fracture of a plate with the expansion of a gas cavity in water," *J. Appl. Mech. Tech. Phys.*, **32**, No. 5, 802–807 (1991).
21. M. A. Lavrentyev and B. V. Shabat, *Problems of Hydrodynamics and Their Mathematical Models* [in Russian], Nauka, Moscow (1973).
22. S. K. Godunov and N. N. Sergeev-Al'bov, "Equations of the linear theory of elasticity with point Maxwellian sources of stress relaxation," *J. Appl. Mech. Tech. Phys.*, **18**, No. 4, 549–560 (1977).
23. E. I. Romenskii, "Method for calculating two-dimensional dynamic equations of a Maxwellian nonlinear elastoplastic medium," Preprint No. 36, Inst. Mathematics, Sib. Div., Acad. of Sci. of the USSR, Novosibirsk (1988).
24. L. M. Kachanov, *Foundations of the Theory of Plasticity*, North-Holland, Amsterdam–London (1971).
25. Yu. N. Rabotnov, *Mechanics of a Deformable Solid* [in Russian], Nauka, Moscow (1988).